GPS monitoring of the tropospheric water vapor distribution and variation during the 9 September 2002 torrential precipitation episode in the Ce´vennes (southern France)

Cédric Champollion, Frédéric Masson, Joël van Baelen, Andrea Walpersdorf, Jean Chéry, Eric Doerflinger

GPS monitoring of the tropospheric water vapour distribution and variation during the September 9, 2002, torrential precipitation episode in the Cévennes (Southern France)

C. Champollion (1), F. Masson (1), J. Van Baelen (2), A. Walpersdorf (3), J. Chéry (1), E. Doerflinger (1)

(1) Laboratoire Dynamique de la Lithosphère, Université Montpellier II - CNRS, Montpellier, France (cedric.champollion@dstu.univ-montp2.fr)

(2) Laboratoire de Météorologie Physique, CNRS – Université Blaise Pascal, Clermont-Ferrand, France

Formerly with: CNRM/GAME, CNRS - Météo-France, Toulouse, France

(3) Laboratoire de Géophysique Interne et Tectonophysique, Université Joseph Fourier – CNRS, Grenoble, France

Corresponding author: Cédric Champollion

Abstract

On September 8-9, 2002, torrential rainfall and flooding hit the Gard region in southern France causing extensive damages and casualties. This is an exceptional example of a so called Cévenol episode with 24h cumulative rainfall up to about 600 millimetres at some places and more than 200 millimetres over a large area (5500 km²). In this work, we have used GPS data to determine Integrated Water Vapour (IWV) as well as horizontal wet gradients and residuals. Using the IWV, we have monitored the evolution of the convective system associated with the rainfall from the water vapour accumulation stage through the stagnation of the convective cell and finally to the break-up of the system. Our interpretation of the GPS meteorological parameters is supported by synoptic maps, numerical weather analyses and rain images from meteorological radars. We have evidenced from GPS data that this heavy precipitation is associated with ongoing accumulation of water vapour, even through the raining period, but that rain stopped as soon as the weather circulation pattern changed. The evolution of this event is typical in the context of the Cévenol meteorology. Furthermore, we have shown that the horizontal wet gradients help describe the heterogeneity of the water vapour field and holds information concerning the passage of the convective system. Finally, we have noticed that the residuals, which in theory should be proportional to water vapour heterogeneity, were also highly perturbed by the precipitation itself. In our conclusions, we discuss the interest of a regional GPS network for monitoring and for future studies on water vapour tomography.

Keywords: GPS, water vapour, wet gradients, intense rainfall, Integrated Water Vapour, residuals.

1. Introduction

In autumn, southern France along the Mediterranean arc is regularly the theatre of extreme precipitation and flooding events producing societal damages including public and private goods destruction but also sometimes loss of lives. Such a strong event took place on September 8-9, 2002 in the Gard region. It can be categorised as a centennial catastrophe given the amount of precipitation and the extent of flooding. Indeed, the maximum value of daily accumulated precipitation recorded for the 8th of September is 543 mm at Saint-Christol-lès-Alès in the Gard department, while the heavy precipitation occurred mainly in the afternoon of that day and the following night. Such a value is close to the actual mean accumulated precipitation over a year for that region. Furthermore, the geographical extent of the rainfall is extremely large as shown in figure 1, where an area of about 5000 km^2 received an accumulated amount of precipitation of more that 300 mm for a 48 hour period. Finally, the September 8-9, 2002 event accounts for a human loss of life of 13 plus 6 missing, while property damages add up to several tens of million Euros.

This heavy precipitation event followed the classical development scheme associated with the so-called “Cévenol episodes” named after the Cévennes region which lies between the Massif Central mountainous region and the Mediterranean plains. In this scheme (Barret et al., 1994), a deep trough positioned between Ireland and Portugal generates a stationary cut-of-low positioned over Spain associated with cold stratospheric intrusion in altitude and a strong jet circulation which will produce lifting at its exit positioned over the Cévennes region. Meanwhile, a surface low develops over the Mediterranean Sea which induces a southern low level flux of warm and humid air in the lower layers of the atmosphere. Thus, the encounter of the cold altitude air with the warm and humid surface flux plus the forcing due to the jet and the orography (the rise of the Massif Central and the funnelling effect between those mountains and the pre-Alps to the east) produces a very unstable atmosphere prone to initiate deep convection and associated strong precipitation. Autumn is such a critical period because the artic cold air in altitude associated with

the trough formation often reaches these latitudes for the first time after the summer and come across a warm Mediterranean sea and coastal regions. Hence, more than 70% of rain events with more that 200 mm daily accumulated precipitation take place between August 25 and November 15 in that region (Barret et al., 1994).

The societal impact of such events could be strongly mitigated if better forecasts of the expected amount of precipitation and its location were available. Usually, the main limitation for an accurate prediction of the precipitation and the modelling of the rain event dynamics is the poor knowledge of the water vapour field initial distribution and evolution (Emanuel et al., 1995; Ducrocq et al., 2002). Indeed, although the amount of water vapour cannot be directly linked to precipitation amounts, water vapour can fuel the corresponding convective process.

Nowadays, to measure water vapour in the atmosphere, meteorological services rely on standard synoptic radiosoundings. However, even though such devices provide reasonably accurate measurements of water vapour profiles, they are far too sparsely distributed in space and time to support reliable forecasting of such rain events. Lately, Global Positioning Systems (GPS) has demonstrated its ability to monitor integrated water vapour (IWV) (Businger et al., 1996; Duan et al., 1996, Tregonning et al., 1998) with an accuracy comparable to other means of measurements (radiosoundings, microwave radiometers, …) (Niell et al., 2001; Revercomb et al., 2003; Van Baelen et al., 2004), but also with good time resolution (better than hourly) and under all meteorological conditions. As more and more GPS are being deployed and operated in a continuous mode for geodetic purposes, they offer the potential for a dense and reliable water vapour measurement network. In this study, we have used the data collected by continuously or semi-continuously operating geodetic and geodynamical networks in Southern France as well as some reference GPS stations in Europe.

In the following sections, we will first introduce the GPS data used and their processing before focussing on the derivation of those parameters relevant to the meteorological documentation of the atmospheric water vapour content, distribution and variation. Then, we will present the meteorological context of this event. We will study the IWV distribution and

evolution during the event while considering the associated rainfall. From the wet gradients and the residuals, we will describe the variability of the water vapour in the convective system. Furthermore, the effect of heavy rain on the GPS signals will be shown by a careful study of the residuals of the GPS processing. Finally, we will draw our conclusions and discuss the applications of GPS for weather monitoring and tomographic studies.

2. GPS data and processing

The GPS data used in this study come from the continuously operating French networks RGP (Nation-wide permanent GPS network from the Institut Géographique National: http://lareg.ensg.ign.fr/RGP/RGPhome.html) and REGAL (Alpine region GPS geodetic network: http://kreiz.unice.fr/regal), from the continuously operating GPS network of Catalonia CATNET (http://draco.icc.es/geofons/catnet/en/home.php), and from 3 GPS stations of the semi-continuously operating French network VENICE (Masson et al., 2002). The GPS station MAHO in the Balearic Islands is maintained by the Royal Observatory of Spain. The geographical spread and density of those GPS stations is quite sparse but allows for the monitoring of the water vapour distribution and variations from the Balearic Islands in the Mediterranean Sea to the Alps and over the area of heavy precipitation and flooding.

The GPS data processing was performed with the software GAMIT/GLOBK (King and Bock, 2000) in a quite conventional way. We compute in a first run the precise coordinates of the GPS stations in the ITRF 2000 frame (Altamimi et al., 2002) using 24 hour sessions, a cut-off angle of 10° and IGS final orbits. We use 10 GPS stations in Europe for the frame referencing. The final station coordinates are obtained by constraining the fiducial GPS stations to their ITRF2000 coordinates using the Kalman filter GLOBK (Herring et al., 1990) in a global solution. We find a repeatability of about 2 mm on horizontal and 5 mm on vertical baseline components. Then we perform a second run with loose constraints of 1 meter on the coordinates to evaluate

hourly the tropospheric parameters (Bock et al., 2003) i.e. the Zenith Total Delay (ZTD) and the total gradients. The lengths of the baselines are more than 1500 km to decorrelate the tropospheric parameters estimation from vertical positioning. The zenith delay a priori constraints, the variation of the Gauss-Markov process and the correlation time were set to 0.5m, 0.01 m/√h and 100 h respectively and for the gradients 0.01 m, 0.01 m/√h and 100 h. Once again we use the IGS final orbits. We choose the "dry" and "wet" mapping functions described by Niell (1996). We apply a sliding window session of 24 hours shifted by 12 hours to suppress the edge effect using the middle 12 hour of the session. The atmospheric parameters calculated during the GPS treatment are the ZTD, the North-South and the East-West total gradients at the elevation of 10°.

3. Wet delay, gradients and one-way residuals

The total atmospheric delay $\boldsymbol{L_{atm}}$ between a GPS receiver and each visible satellite is a function of both the elevation angle $\boldsymbol{\varepsilon}$ and the azimuth angle $\boldsymbol{\alpha}$. Following Chen and Herring (1997), it can be decomposed into a spherically symmetric contribution of the atmosphere $\boldsymbol{L_{sym}}$, an azimuth dependent contribution of the atmosphere due to its anisotropy $\boldsymbol{L_{az}}$, and residuals ***S:***

$$L_{atm} = L_{sym}(\varepsilon) + L_{az}(\varepsilon,\alpha) + S \quad (1)$$

with

$$L_{sym(\varepsilon)} = L_h^z m_h(\varepsilon) + L_w^z m_w(\varepsilon) \quad (2a)$$

$$L_{az}(\varepsilon,\alpha) = L_h^{ns} m_{az}(\varepsilon)\cos(\alpha) + L_h^{ew} m_{az}(\varepsilon)\sin(\alpha) + L_w^{ns} m_{az}(\varepsilon)\cos(\alpha) + L_w^{ew} m_{az}(\varepsilon)\sin(\alpha) \quad (2b)$$

$L_{sym}(\varepsilon)$ is only elevation dependent. $\boldsymbol{L_h^z}$ and $\boldsymbol{L_w^z}$ are the zenith hydrostatic and wet delay, respectively, while $\boldsymbol{m_h(\varepsilon)}$ and $\boldsymbol{m_w(\varepsilon)}$ are the corresponding hydrostatic and wet mapping functions. In this study, we use the Niell mapping functions (Niell, 1996). $L_{az}(\varepsilon,\alpha)$ is azimuth and elevation dependent. $\boldsymbol{L_h^{ns}}$, $\boldsymbol{L_h^{ew}}$, $\boldsymbol{L_w^{ns}}$ and $\boldsymbol{L_w^{ew}}$ are respectively the north–south and east–west components of the hydrostatic and wet gradients. $\boldsymbol{m_{az}}$ is the gradient mapping function defined by Chen and Herring (1997). Residuals $\boldsymbol{S}$ are then defined as the difference between the GAMIT final model results and the observations (using the ionosphere free linear combination LC). The ZTD obtained during the GPS treatment with the GAMIT software is the sum of $\boldsymbol{L_h^z}$ and $\boldsymbol{L_w^z}$ at the zenith or $L_{sym}(90°)$. The North-South and the East-West gradients calculated by the GAMIT software are respectively $L_{az}(10°,0°)$ and $L_{az}(10°,90°)$.

In order to study the water vapour contribution to the GPS signals, we have to extract the wet delays and gradients from the total atmospheric delay and gradients. To do so, we first derive the hydrostatic part of the zenith delay ($\boldsymbol{L_h^z}$) from surface pressure measurements (Figure 2a) interpolated at the station position following Davis et al. (1985). The surface pressure measurements are the hourly synoptic observations of Météo-France (French National Weather Service). The accuracy of the pressure measurement is 0.1 hPa. The hydrostatic part of the total gradients (Figure 2b) is calculated from spatial variations of the ground pressure. From the pressure field near the GPS station, we calculate the spatial variations of the hydrostatic delay per unit of distance (km) in the north-south and east-west directions: $\boldsymbol{Z_h^{ns}}$ and $\boldsymbol{Z_h^{ew}}$. Thus, the equations for the hydrostatic gradients $\boldsymbol{L_h}$ and for the spatial variations of the hydrostatic delay $\boldsymbol{Z_h}$ are:

$$L_h = \int_0^\infty z.g(z)dz \qquad \text{and} \qquad Z_h = \int_0^\infty g(z)dz \qquad (3a \ \& \ 3b)$$

where $\boldsymbol{g}$ is the horizontal gradient of the dry refractivity. Following Flores et al. (2000) or Elosegui et al. (1999), we convert $\boldsymbol{Z_h}$ to the hydrostatic gradients $\boldsymbol{L_h}$ assuming an exponential law in the hydrostatic refractivity such that:

$$L_h^{ns} = H.Z_h^{ns} \qquad \text{and} \qquad L_h^{ew} = H.Z_h^{ew} \tag{4}$$

where $\boldsymbol{H}$, the scale height of the gradients in the hydrostatic delays is set to 13 km following Chen and herring (1997), who propose a larger scale height for the gradients than those normally associated with the atmosphere, although they recognize that this assumption still needs to be confirmed by atmospheric simulation tests with a non-hydrostatic model.

The effect of the hydrostatic gradient correction seems to be negligible in normal atmospheric conditions. On the contrary, during the passage of the convective system over the area during the studied event, the hydrostatic gradient amounts to about 20 % of the total gradient which is not negligible (figure 2b). Furthermore, the hydrostatic gradient is opposite to the total gradient, indicating that we need to take into account the hydrostatic gradient in order not to underestimate the wet gradient.

Removing the hydrostatic contributions from the total delay leaves us with the zenith wet delay which can be converted into Integrated Water Vapour (IWV) using the formula obtained for the Mediterranean area by Emardson and Derks (1999) from more than 37000 radio-soundings and temperature surface measurements:

$$\frac{L_w}{I} = a_0 + a_1.T_\Delta + a_2.T_\Delta^{\,2} \tag{5}$$

where $\boldsymbol{L_w}$ is the "wet" delay, $\boldsymbol{I}$ the Integrated Water Vapour (IWV), $\boldsymbol{T_\Delta}$ the surface temperature minus the mean surface temperature of the area (289.76 °K for the Mediterranean area) and $\boldsymbol{a_0, a_1, a_2}$ coefficients derived by Emardson and Derks (1999) (respectively 6.324, -0.00177 and 0.000075). The accuracy of the equation (5) is estimated by the authors to be approximately 1%.

The IWV represents the mean zenith integrated water vapour as seen by one GPS station and depends on the spatial distribution of the satellites. Typical amplitudes of the IWV are between 5

and 40 kg/m² with an accuracy of about 1 kg/m² compared to VLBI, radio sounding and radiometer (Niell et al., 2001). The Wet Gradients represent the integrated linear heterogeneity of the water vapour above the GPS station in the direction of those satellites. The accuracy of the Wet Gradients is still poorly defined as the wet gradient is a parameter characteristic of GPS which is difficult to reproduce with other instruments like the radiometer (Gradinarsky et al., 2000). The post-fit residuals are the one-way (station-satellite) phase differences between the model obtained from GAMIT by least square inversion and the observations. During "normal" atmospheric conditions, they are mainly due to multi-path, uncorrected phase centre variations and receiver clock error and thus they can not be interpreted in terms of water vapour content. The magnitude of the residuals is about 1 mm of delay at the zenith. During particularly dynamic meteorological conditions, local atmospheric heterogeneities or hydrometeors can greatly enhance these residuals (as shown later in section 7.).

4. Meteorological context of the 8-9 September 2002 rain event.

To study the meteorological background of this event, we will use 500 hPa geopotential analysis maps (Figure 3), surface wind and temperature analysis maps (Figure 4) and rain images (Figure 5) from the meteorological radar located near the town of Nîmes, France. The beam of the radar is 1.8°. Each image is calculated from 3 scans at 0.6°, 1.3° and 2.5° elevation above the horizon.

Figure 3 shows the 500 hPa geopotential analysis maps for Sunday 8 September and Monday 9 September 2002 at 12:00 UTC. On the Sunday 8 September (Figure 3a), an upper cold pressure low is extended from Ireland to Spain by a deep trough. The low-level circulation associated to this low pressure on the Iberian Peninsula is a warm and moist south flow in the South France and in the Rhône Valley. This surface circulation is clearly seen on the Météo France operational model ARPEGE analysis surface maps on Figure 4a. The convection starts on the Mediterranean Sea (04 UTC) as seen on the rain radar images (Figure 5a) and in the land in the morning (Figure 5b). This deep convection organises itself in a V-shape, typical for high

precipitation event in French Gard area (Figure 5c). The edge of the V is positioned at the place of maximum convection where the clouds elevate the highest and where the precipitation is maximum. The clouds develop down-stream in a V shape fashion (Figure 5c) along the Massif Central contours and across the Rhône valley (Barret et al., 1994). The orientation of the V-shape is given by the South-Western diffluent winds at the tropopause level (Figure 3a-b). This deep convective system will give the main part of the precipitation. During the afternoon and the night of the 8 September, the region of precipitation moves slowly towards the East (Figure 5d).

On Monday 9 September in the morning, the arrival of warm air from the Mediterranean Sea is still active (Figure 4b). Then, in the afternoon (Figure 3b), the axis of the trough changes from roughly North to South to North-West to South-East. The low-level flow begins to decay (Figure 4c) and the convection cells move towards the East (Figure5 e-f). The change in the synoptic circulation corresponds to the end of the high precipitation in the south of France. More detailed description of the event and of the associated precipitation can be found in Delrieu et al. (2004). This event associated with deep stationary convection above the Gard region caused the historical precipitation described in the introduction and represented on the figure 1.

5. IWV variations and associated rainfall

5.1 Description of the IWV time series

Figure 6 shows the temporal variation of the IWV from September 7th to September 9th (days 250 to 252) 2002, at selected stations used in our analysis. The initial amount of water vapour is high around the Balearic Islands (30 kg/m² in MAHO, day 250 12 hours UT), increases going to the north (35 kg/m² in CREU, day 250 18 hours UT) and is maximum in MTPL (40 kg/m², day 251 12 hours UT) close to the rainfall. Hence, during the south to north travel, the air is continuously loaded with water vapour from evaporation due to the Mediterranean Sea high surface temperatures at this period of the year (Figure 4 and Delrieu et al., 2004). As the stations MAHO, CREU and MTPL are situated on the flux trajectory, one can notice that the water vapour maximum is shifted by about 6 hours between MAHO and CREU, while between CREU

and MTPL the shift takes about one day indicating the stagnation of the mass of humid air which creates the favourable conditions for sustained convection.

Four groups of stations can be distinguished. First, the south-western stations (group 1: MALL, MAHO, EBRE, BELL and CREU), from the Balearic Islands to the Eastern Pyrenees which document the inflow to the precipitation area; second, the stations on the western border of the core of the precipitation area (group 2: MTPL, AIGL); third, the stations to the east of the precipitation area, at the foothills of the pre-Alps mountains (group 3: CHRN, MARS, VERC, SJDS, MICH, GINA); and finally, the stations in the exit part of the convective system, further to the east and the north (group 4: SJDV, JOUX, FCLZ, GRAS, SOPH, AJAC).

Considering the Group 1 one can easily notice the increase of IWV during the day 250 of about 10-15 kg/m². One notices as well its south to north progression in time and amplitude. Both are expected with the southern flow from the Mediterranean Sea (Figure 4). The IWV remain high during the end of the day 250 and the day 251. These stations within and around the Mediterranean Sea are located in the region of water vapour loading of the atmosphere: the area of convergence of water vapour of the south low-level flux (Figure 4). Around the western border of the rainfall zone, the group 2 shows an increasing IWV not only during the day 250 but also during the day 251. The increase from 20 to 40 kg/m² of the IWV is spectacular for the MTPL station. This station location can be considered as the southern limit of the catastrophic rainfall event and demonstrates the high water vapour accumulation in that region prior to the start of the precipitation. Likewise, the AIGL station, which is in altitude on the first slopes of the Massif Central, exhibits relatively high values of IWV corresponding to the ascent of water vapour loaded convective clouds upon the orography (Figure 5c). The group 3 located on the eastern border of the zone of the catastrophic rainfall does not show a clear evolution of the IWV on day 250 up to the morning of day 251 and a very abrupt increase of the IWV at about 06 UTC on day 251. This indicates that there is no water vapour loading in that region: IWV increases only when the convective system expands over those stations. One will notice that the observed step of 10 kg/m² for the group 3 is generally preceded by a slight decrease of the IWV. Most of the

precipitation has been observed between the groups 2 and 3 where, unfortunately, no GPS permanent station was operating during this period. The contrasted IWV behaviour between these two last groups (2 and 3) fits the common description of Cévenol episodes with V shaped convective cloud formations. In our case, the group 2 are in the up-stream of the convective cell and monitor the build-up of water vapour and fuelling of the system. The group 3 shows a decrease of water vapour probably associated with low level convergence to the edge of the system at the time of convective initiation, and a later increase of water vapour corresponding to the development of the convective clouds above their region. Therefore, as demonstrated in figure 2b, those stations of the group 3 will also experience a strong East to West wet gradient with higher values of IWV to the west, within the convective cloud build up zone during the day 251 above the Gard region. Finally, the stations of group 4 show signs of two parts of the event. Its Mediterranean sites exhibit, to a lesser proportion, some water vapour increase associated with the southern flux of warm and humid air (Figure 4). Its northern sites show signs of fairly perturbed but high levels of water vapour associated with the exit phase of the convective region during the night of 8 to 9 of September and the following day. For comparison, the water vapour variation at the GRAZ station in Austria is also shown to illustrate unperturbed meteorological conditions during those three days of the study.

In a processing point of view, the similarity and simultaneity of the transition for all those stations located in a very small area is a good indication of the quality of the IWV estimates.

5.2 Spatial evolution of the IWV

To support the analysis above, we will now consider the evolution of the water vapour field revealed by successive IWV maps (Figure 7) over the area of interest. In order to plot the spatial variation of the IWV content corrected for the effect of altitude (the altitude of the GPS stations varies from sea level to more than 1500 meters high in the Cévennes or in the Pyrenees), we plot the IWV relative to a reference distribution chosen at the beginning of the event: day 250 at 03 UTC. The IWV maps obtained are determined by Hermit interpolation over the whole network.

Hermit interpolation uses the value and their derivatives in each point of measure to constrain a polynomial interpolation. In this case, we use the east-west and north-south wet gradients as the horizontal derivatives of the IWV values. Thus, using Hermit interpolation the IWV variations are well defined even in the areas without GPS stations but surrounded by several GPS stations. This is the case for the Gard department which corresponds to the region of maximum rainfall. Inversely, the borders of the map are noisier due to a lack of neighbouring data.

Although the GPS network is quite sparse, the large-scale spatial and temporal variations can be studied from the IWV spatial distribution maps. They clearly point out the water vapour displacement from the Mediterranean Sea (Figure 7a) to southern France and its accumulation over the Gard region. The high water vapour zone is limited to the west by the line CREU-MTPL, on the east by the line MARS-MICH and on the north by the station SJDV. This indicates that the area of high water vapour content is larger than the area of heavy precipitation as previously shown in figure 1. The maximum IWV is located in the Gard region during about 24 hours between 06 UTC day 251 and 06 UTC day 252 (Figures 7b-d) and is well correlated with the area and period of maximum precipitation. At 12 UTC on day 252, the water vapour flux from the south becomes weaker and its orientation changes, the water vapour and the convective cell move towards the east (Figures 7e-f) indicating the end of the stagnation and the dilution of the convective system. All these characteristics are well correlated with the rain images from Météo-France radars, especially the eastward motion of the rain system which marks the end of the catastrophic event (Figure 5).

5.3 Correlation between IWV and rain

To investigate the correlation between IWV and rain at the ground level we will look at those GPS stations closest to the core of precipitation (AIGL, MTPL and CHRN) and which were almost collocated with raingauges (less than 5 km). Raingauges provide hourly accumulated precipitation data. The most intense rainfall has been recorded at the AIGL GPS station, with a maximum of 50 mm/h at midnight on day 251. IWV and rainfall temporal variations do not show

any clear correlation (Figure 8a). The increase of IWV is regular while the rain is abrupt. The maximum of IWV (30 kg/m²) occurs at the end of the rain time in early morning of day 252. It is interesting to point out that the increase of IWV continues during the rain. In MTPL (Figure 8b), the rainfall is less abrupt than in AIGL (25 mm/h) but spreads over a longer period (about 12 hours). Once again there is a continual increase of water vapour during the rain and a maximum IWV at the end of the rain. This could indicate that the decrease of water vapour due to the precipitation is overcompensated by the south flux of water vapour which fuels the convective system and by evaporation. The measured rain at CHRN is quite different (Figure 8c). We see a high increase of IWV on the beginning of the day 251 followed by a small rain event (20 mm/h) at noon. This is comparable to the phenomena observed at MTPL but with less intensity. However, a stronger rain event (30 mm/h) is observed later at about 6 UTC on day 252 and is directly correlated to a short term increase of water vapour. This is to be linked with intense but localised precipitation which can arise in the wake of the V-shape convective system that has developed over the Gard region and has far less impacts than the large and continuous rain experienced at the core of the system. To summarize, the large rain event occurred when the IWV reached high values of about 30 to 40 kg/m² (water vapour fuels the convective system) but there is no direct relationship between IWV and the amount of precipitation.

6. Heterogeneity of water vapour distribution: study of wet gradients

As the poor density of the GPS network available does not allow for detailed studies of the water vapour heterogeneities based on the IWV only, we will now study the meteorological information provided by the sum of the wet gradients and the residuals. It can be viewed as an accurate description of the horizontal heterogeneities of the atmosphere within the GPS station field of view.

The sky plots in figure 9 show the sum of the wet gradients and the residuals for the CHRN station during the day 252 for a period of 4 hours, while the black arrows represent the mean gradient and the ellipses its dispersion (RMS) during the corresponding periods. On these sky plots, one can easily observe the motion of the IWV associated with the convective precipitation event studied. From 0 to 8 UTC, the gradients reveal a high concentration of water vapour towards the west and the south. The sky plots show a clear East to West pattern, involving a relatively high gradient and a small RMS. This is consistent with the stagnation of the convective system over the Gard region (to the west) and its fuelling with water vapour coming from the Mediterranean (to the south). From 8 to 16 UTC, the gradients do not show any clear pattern and their RMS over four hours becomes larger than the signal. This can be related to the convective system extending above the station considered and filling the GPS field of view. After 16 UTC, there is a clear (but small) west to east pattern in the sky plots. The corresponding west to east gradient associated with a small RMS is opposite to the gradient in the morning. This can be related to the fact that the convective system has broken up and is being advected further to the east. Observations from the other GPS stations in the vicinity of the heavy rainfall area are all consistent with the water vapour evolution scheme just described. Moreover, the water vapour evolution depicted here compares favourably with the meteorological radar observations of the rain system (Figure 5). Finally, one will also notice that the maximum amplitude of the wet gradients is not correlated with the rain itself. Actually, rain seems to occur when there are rapid changes in both the orientation and the amplitude of the wet gradients.

In summary, the information provided by the wet gradients is a quasi-direct measure of the water vapour field horizontal variability within a horizontal scale of about 50 km. Thus, a GPS station is capable not only to provide an observation of the integrated water vapour content of the troposphere above the receiver but can also provide a numerical measure of the azimuth variation of the water vapour distribution.

7. Investigation of the residuals

To get a more detailed look at the water vapour heterogeneity, we will now consider the residuals in an isolated way. Compared to the wet gradients, the residuals could provide the finest scale heterogeneity (less than 50 km) of the water vapour field. They are not a mean model of the heterogeneity over all the satellites like the gradients but the remaining signal between one GPS station and one satellite. On the figure 10, we have plotted the sky plots of the residuals along the GPS satellites tracks for the 8 September at MTPL (Julian day 251 of 2002). During the main rainfall from 8 to 20 UTC, the residuals are high and variable. Compared to average values of the residuals at this station, the residuals observed during the rainfall are two to three times larger. However, they do not allow identifying any water vapour organised structure. These high residuals do not result from multipath either as they are not elevation dependent. They could be due to an increase of electromagnetic (EM) effects of the fibreglass box of the GPS antenna during the rain. Indeed, the water on the fibreglass box could change its EM characteristics. But if that was the case, the rain should only enhance pre-existing patterns of the residuals (Herring and Shimada, 1999) and that is not verified here. Another explanation could be a large and very high temporal variability of the water vapour during the rain with some interaction between evaporation and condensation. To test this hypothesis, we compute gradients and ZTD every 30 and 15 minutes to have a finer representation of the temporal variation of water vapour field. If the temporal variability of the troposphere was the main reason for those residuals, they should decrease using shorter meteorological GPS parameter intervals. We find only a limited decrease of the residuals but not strong enough to retrieve the typical amplitude of a normal day at these stations or of another GPS station (WTZR) in central Europe (table 1). The unmodelled spatial variability of water vapour within the field of view of the GPS antenna could also contribute to the residuals. This kind of hypothesis could be tested with a local tomography of water vapour (Champollion et al., 2004). The tomography can however not be achieved for this study because of the too large spacing between GPS stations. Finally, the most significant part of the residuals could be due to liquid water in the troposphere in the form of rain, ice and clouds. The

enhancement of the residuals is well correlated in time with the precipitation with a maximum for MTPL and CHRN at about 12 UTC the 8 September. The levels of residuals found in our study are in good agreement with the absorption model described by Solheim et al. (1999) who find 5 mm/km of surface delay for rainfall of 50 mm/h with a scale height of 3 or 4 km. Further studies with high resolution numerical weather simulations confirm this hypothesis (Brenot *et al*., 2004).

8. Conclusions

IWV temporal variations (Figure 5), IWV spatial variations (Figure 6) and wet gradients temporal variations (Figure 9) can improve the understanding of large rainfall events. They allow an accurate and continuous description of the water vapour field variations before, during and after the heavy precipitation.

In our case study, the IWV reveals that the water vapour flux is initiated in the Mediterranean Sea south of the Balearic Islands and moves northward parallel to the Spanish shoreline. The water vapour content increases during the northward motion. The velocity of the flux decreases while reaching the French shoreline. Finally, the maximum water vapour content is observed in MTPL, just south of the maximum rainfall zone. Different temporal variations of IWV are observed between the GPS stations west and east of the rainfall area. The water vapour increases continuously and linearly for the stations south-west of the raining area. They are located in the 'loading' zone. East of the raining area, the IWV variations are more complex, with successive increases and decreases, indicating the complexity of the phenomena close to the rainfall zone at time of precipitation but especially once the convective system breaks up. These interpretations are confirmed by the ARPEGE analyses and the rain images from radars (Figure 4 and Figure 5).

This study also illustrates an important result about the Wet Gradients: a single GPS station can provide partial information on the heterogeneity of the troposphere by extracting the wet gradients. During the passage of the rain system, the wet gradients are weak and highly variable.

Before and after the rain, the wet gradients give clear information of the lateral heterogeneity of the atmosphere. They indicate the contrast of humidity between the different parts of the meteorological system. For the monitoring of air mass heterogeneity, the wet gradients are a good indicator which could be available in near real time like other meteorological parameters. They could be used for estimating the time of arrival of a front above a GPS station and, thus, for checking and updating the event chronology in numerical weather prediction forecasts.

Theoretically, the study of the residuals provides the finest information about the water vapour heterogeneity which cannot be modelled by the IWV and the gradients. The residuals also include the noise due to the liquid water, the multipath, the errors of the mapping function, etc. The MTPL data indicate that the residuals increase significantly during the large rainfall probably due to rain scattering. If this observation is confirmed, GPS residuals could be investigated in relation with the characterisation of the rain. Furthermore, the modelling of the residuals due to the rain could be useful to correct the gradients for meteorological applications like GPS water vapour tomography (Champollion et al., 2004) or data assimilation in numerical models (Gutman et al., 2004).

This study has been conducted using the current permanent GPS network of southern France and Spain. Further studies need a denser GPS network recording data during a long period to get a database covering several catastrophic rainfall events. A large database will allow to characterize the catastrophic rainfall situations and to distinguish these events from standard autumnal precipitation. A field experiment could be conducted next autumn with more temporary GPS stations from Marseille to Agde, i.e. covering the zone of the maximum rainfall with a typical spacing of 50 km. From these data, we will be able to resolve the small scale variations in 3D of the water vapour with the tomographic software we have developed (Champollion et al., 2004) and get an insight into monitoring and the dynamics of strong rain events. GPS stations have been located close to the shoreline to study the potential of GPS to explore the troposphere above the Mediterranean Sea, to provide a precursor of the catastrophic rainfall events. In ongoing work, gradients and residuals will be carefully studied.

Acknowledgments

This work was partially supported by the Institut des Sciences de la Terre, de l'Environnement et de l'Espace de Montpellier (ISTEEM) and by the Observatoire Hydro-météorologique Méditerranéen Cévennes-Vivarais (OHMCV). We thank Philippe Collard, Laboratoire Dynamique de la Lithosphère (LDL) for his work in the installation and the maintenance of the VENICE semi permanent GPS network, Sandrine Anquetin and Simon Yates, Laboratoire d'étude des Transferts en Hydrologie et Environnement (LTHE) for providing the raingauge data. We would like to thank the three anonymous reviewers for their detailed and relevant comments of this paper.

REFERENCES

Altamimi, Z., P. Sillard, and C. Boucher, ITRF2000: A new release of the International Terrestrial Reference Frame for earth science applications., J. Geophys. Res., 107, B10, 2002.

Barret, I., V. Jacq, and J-C. Rivrain, Une situation à l'origine de pluies diluviennes en région méditerranéenne, La Météorologie, 8, 7, 38-60, 1994.

Bock, O., M.-N. Bouin, Y. Morille, and T. Lommatzsch, Study of the sensitivity of ZTD estimates to GPS data analysis procedure, EGS XXVII, Nice, 2003.

Brenot, H., V. Ducrocq, C. Champollion, and A. Walpersdorf, Zenith delays sensitivity evaluate from electromagnetic GPS signal's propagation in a high resolution N.W.P. during the 8-9 September 2002 event., J. Geophys. Res., in preparation, 2004.

Businger S., S.R. Chiswell, M. Bevis, J. Duan, R.A. Anthes, C. Rocken, R.H. Ware, M. Exner, T. VanHove, and F. Solheim, "The promise of GPS in atmospheric monitoring". *Bull. Amer. Meteor. Soc.*, vol. 77, pp. 5-18, 1996.

Chen, G., and T. A. Herring, Effects of atmospheric azimuthal asymmetry on the analysis of space geodetic data, J. Geophys. Res., 102, B9, 20489-20502, 1997.

Champollion, C., F. Masson, M.-N. Bouin, A. Walpersdorf, E. Doerflinger, O. Bock and J. Van Baelen, GPS Water Vapour Tomography: First results from the ESCOMPTE Field Experiment, Atm. Res. Accepted, 2004.

Davis, J. L., T. H. Herring, I. I. Shapiro, A. E. E. Rogers, and G. Elgered, Geodesy by radio interferometry: Effects of atmospheric modeling errors on estimatoin of baseline length, Radio Sci., 20, 1593-1607, 1985.

Delrieu, G., V. Ducrocq, E. Gaume, J. Nicol, O. Payrastre, E. Yates, H. Andrieu, P.-A. Ayral, C. Bouvier, J.-D. Creutin, M. Livet, S. Anquetin, M. Lang, L. Neppel, C. Obled, J. Parent-de-Châtelet, G.-M. Saulnier, A. Walpersdorf and W. Wobrock, The catastrophic flash-flood event of 8-9 September 2002 in the Gard region, France: a first case study for the cévennes-Vivarais Mediterranean Hydro-meteorological Observatory, Journal of Hydro-Meteorology accepted, 2004.

Ducrocq, V., D. Ricard, J.-P. Lafore and F. Orain, Storm-Scale Numerical Rainfall Prediction for Five Precipitations Events over France: On the Importance of the Initial Humidity Field, Weather and Forecasting 17, 1236-1256, 2002

Elòsegui, P., J. L. Davis, L. P. Gradinarsky, G. Elgered, J. M. Johansson, D. A. Tahmoush, and A. Rius, Sensing atmospheric structure using small-scale space geodetic networks, Geophys. Res. Lett., 26, 16, 2445-2448, 1999.

Emanuel, K.A., D. Raymond, A. Betts, L. Bosart, C. Bretherton, K. Droegemeier, B. Farrell, J. M. Fritsch, R. Houze, M. LeMone, D. Lilly, R. Rotunno, M. Shapiro, R. Smith, and A Thorpe, Report of the first prospectus development team of the U.S. Weather Research Program to NOAA and the NSF. Bull. Amer. Meteor. Soc., 76, 1194-1208, 1995.

Emardson, T. R., and H. J. P. Derks, On the relation between the wet delay and the integrated precipitable water vapour in the European atmosphere, Meteorological Applications, 6, 1-12, 1999.

Flores, A., G. Ruffini, and A. Rius, 4D tropospheric tomography using GPS slant wet delays, Annales Geophysicae, 18, 223-234, 2000.

Gradinarsky, L. P., R. Haas, Elgered, G. and Jonhasson, J., Wet path delay and delay gradients inferred from microwave radiometer, GPS and VLBI observations, Earth Planets Space 52(10), 695-698,2000.

Gutman, S., S. R. Sahm, S. G. Benjamin, B. E. Schwartz, K. L. Holub, J. Q. Stewart and T. L. Smith, Rapid Retrieval and Assimilation of Ground Based GPS Precipitable Water Observations at the NOAA Forecast Systems Laboratory: Impact on Weather Forecasts, Journal of the Meteorological Society of Japan 82(1B), 351-360,2004

Herring, T. and Shimada, S., GPS Met conference proceedings, Tsukuba-Shi, Japan, Mapping spatial variations in atmospheric delays with GPS. Estimating Spatial Variations in Atmospheric Delays using GPS,
http://www-gpsg.mit.edu/~tah/web/japan_gps_met/GPSMetJapan.html, 1999.

King, R. W. and Y. Bock, Documentation for the GAMIT GPS Analysis Software, release 10.0, Departement of Earth, Atmospheric and Planetary Sciences Massachusetts Institute of Technology-Scripps Institution of Oceanography University of California at San Diego., 2000.

Masson, F., P. Collard, J. Chéry, J.-F. Ritz, E. Doerflinger, O. Bellier, D. Chardon, and M. Flouzat, the VENICE project: a GPS network to monitor the deformation in western Provence and eastern Languedoc (southern France), EGS XXVII, Nice, 2003.

Niell, A. E., Global mapping functions for the atmosphere delay at radio wavelengths, J. Geophys. Res., 101, B2, 3227-3246, 1996.

Niell, A. E., A. J. Coster, F. S. Solheim, V. B. Mendes, A. Toor, J., R. B. Langley, and C. A. Upham, Comparison of Measurements of Atmospheric Wet Delay by Radiosonde, Water Vapour Radiometer, GPS, and VLBI, J. Atmos. Oceanic Technol., 18, 830-850, 2001.

Revercomb H.E., D.D. Turner, D.C. Tobin, R.O. Knuteson, W.F. Feltz, J. Barnard, J. Bösenberg, S. Clough, D. Cook, R. Ferrare, J. Goldsmith, S. Gutman, R. Halthore, B. Lesht, J. Liljegren, H. Linné, J. Michalsky, V. Morris, W. Porch, S. Richardson, B. Shmid, M. Splitt, T. VanHove, E.Westwater, and D. Whiteman, "The ARM program's water vapour intensive observation periods : overview, initial accomplishments, and future challenges", Bull. Amer. Meteor. Soc., vol 84, pp. 217-236, 2003.

Solheim, F. S., J. Vivekanandan, R. Ware, and C. Rocken, Propagation Delays Induceed in GPS signals by Dry Air, Water vapour, Hydrometeors and Other Particulates, J. Geophys. Res., 104, 9663-9670, 1999.

Tregoning P., R. Boers, D. O'Brien, and M. Hendy, "Accuracy of absolute precipitable water vapour estimates from GPS observations", J. Geophys. Res., vol 103, pp. 28701-28710, 1998.

Van Baelen, J., J-P. Aubagnac, and A. Dabas, Comparison of Near Real-Time Estimates of Integrated Water Vapour Derived with GPS, Radiosondes, and Microwave Radiometer, J. Atmos. Ocean. Technol., accepted for publication, 2004.

Tables and Figures

Table 1: Mean RMS of the residuals between 0 and 24 hours UTC, Julian day 251 for the GPS stations MTPL, CHRN and WTZR. The ZTD and Gradients are evaluated every 2 hours, 1 hours, 30 minutes and 15 minutes. The italic numbers indicate respectively the RMS of the residuals between 0-6 UTC, 6-12 UTC, 12-18 UTC and 18-24 UTC. The mean RMS (bold numbers) is for the whole 24 hours.

Figure 1: Map of the 48 hour (from 06 UTC 8 September to 06 UTC 10 September 2002) cumulated rainfall in millimetre in the south of France. The crosses indicate the rain gauges and the black circles the GPS permanent stations. The topography is plotted every 1000 meters with black lines.

Figure 2: a) surface pressure measurement at the sea level the 8 September at 18 hours UT. b) Evolution of the total (circles, dark grey), hydrostatic (triangles, dark grey) and wet (triangles, light grey) gradients at CHRN between the days 250 and 253.

Figure 3: 500 hPa height analyses of Météo-France (French National Weather Service) at 12 UTC the 8 September (a) and the 9 September (b). Geopotentials height (in mgp) and temperature (in °C) are represented respectively by solid and dash lines (H for high center of geopotential and B for low center).

Figure 4: Wind vectors (unit vectors at the top-right of panel corresponding to 25 ms^{-1}) from the ARPEGE analysis at 12 UTC the 8 September (a), 00 UTC (b) and 12 UTC (c) the 9 September.

Figure 5: Map of the rain rates observed by the Nîmes weather radar at 4 UTC (a), 10 UTC (b), 18 UTC (c) the 8 September and at 2 UTC (d), 10 UTC (e), 18 UTC (f) the 9 September 2002.

Black circles indicate the place of GPS stations. On the figure (c), black lines are represented the typical V-shape of rain system.

Figure 6: IWV temporal variations (in kg/m²) during the 7-10 September for selected GPS stations. The absolute IWV map shown corresponds to the first stage of the event (03 UTC the 7 September).

Figure 7: IWV maps of the southeast of France relative to day 250 at 6 PM for each 8 hours from 8 September 2 UT (respectively a, b, c, d, e and f). The topography is plotted every 1000 meters with black lines. On the figure (c), black lines represent the typical V-shape of rain system taken from rain radar images (figure 5).

Figure 8: Temporal variation of the amplitude of the rain (dark grey, in mm) and of the IWV (light grey, in kg/m²) for the Julian days 251-252 at the GPS locations AIGL, MTPL and CHRN (respectively a, b and c).

Figure 9: Sky plot of the Wet Gradients and the residuals along the GPS satellites tracks for the 9 September 2002. Each circle represents a period of 4 hours. The line in the north of the sky plot represents 19 millimetres of delay. Light grey (respectively dark grey) indicates positive (respectively negative) delay. The dark arrow in the centre of each circle represent the mean gradient during 4 hours and the ellipse the associated RMS.

Figure 10: Sky plot of the residuals along the GPS satellites tracks for the 9 September 2002. Light grey (respectively dark grey) indicates positive (respectively negative) delay. Each circle represents a period of 4 hours. The line in the north of the sky plot represents 9.5 millimetres of delay.

Table 1:

	ZTD and gradients evaluated each 2h	ZTD and gradients evaluated each 1h	ZTD and gradients evaluated each 30 min	ZTD and gradients evaluated each 15 min
CHRN	*8.3 9.6 16.1 13.5* **mean: 11.9 mm**	*8.0 9.0 15.8 13.2* **mean: 11.5 mm**	*7.6 8.3 15.5 12.3* **mean: 10.9 mm**	*6.4 7.3 15.3 11.9* **mean: 10.2 mm**
MTPL	*7.2 13.1 22.8 15.7* **mean: 14.7 mm**	7.1 13.1 22.6 15.6 **mean: 14.6 mm**	*6.8 12.1 21.1 14.2* **mean: 13.5 mm**	*6.0 11.1 20.1 12.4* **mean: 12.4 mm**
WTZR	*6.5 5.9 7.8 6.9* **mean: 6.8 mm**	*6.2 5.8 7.3 6.5* **mean: 6.4 mm**	*6.2 5.8 7.3 6.5* **mean: 6.4 mm**	*6.1 5.6 7.3 6.0* **mean: 6.2 mm**

Figure 1:

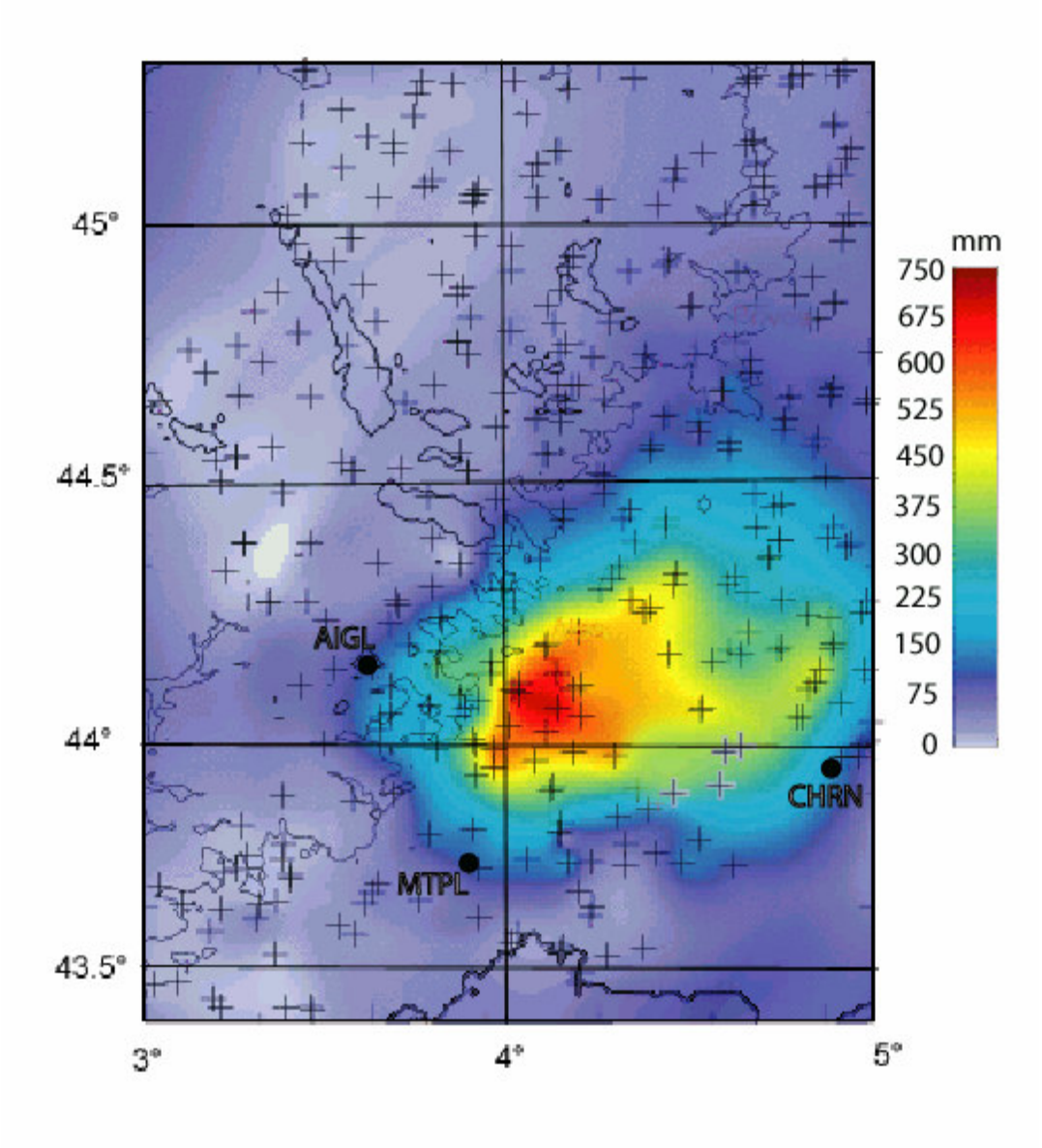
45°
44.5°
44°
43.5°
3°
4°
5°
AIGL
MTPL
CHRN
mm
750
675
600
525
450
375
300
225
150
75
0

Figure 2a:

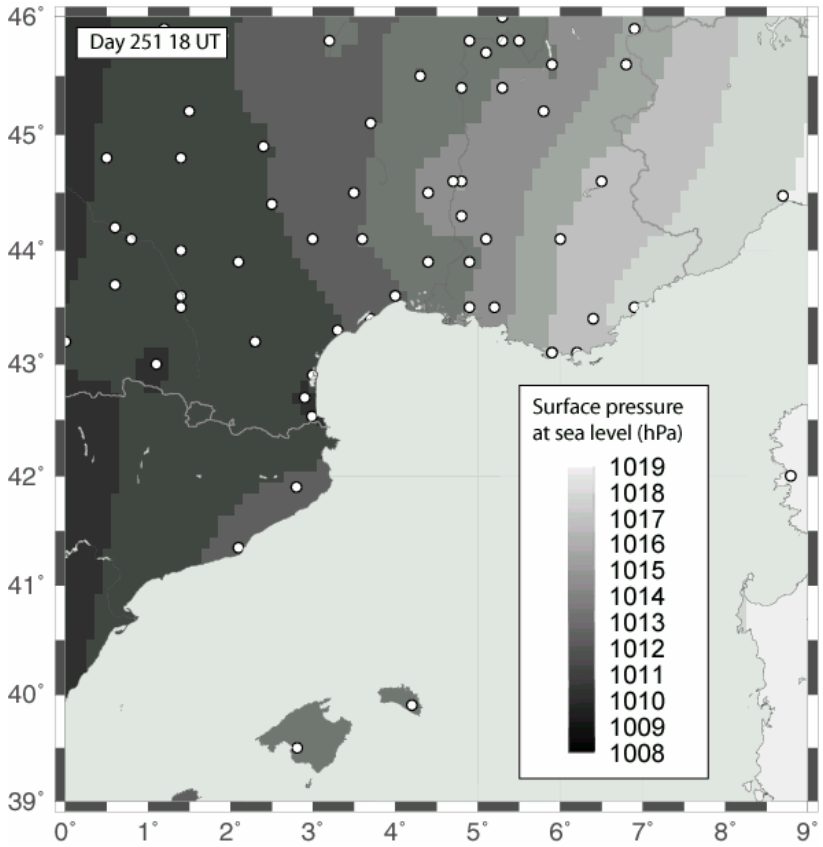

Figure 2b:

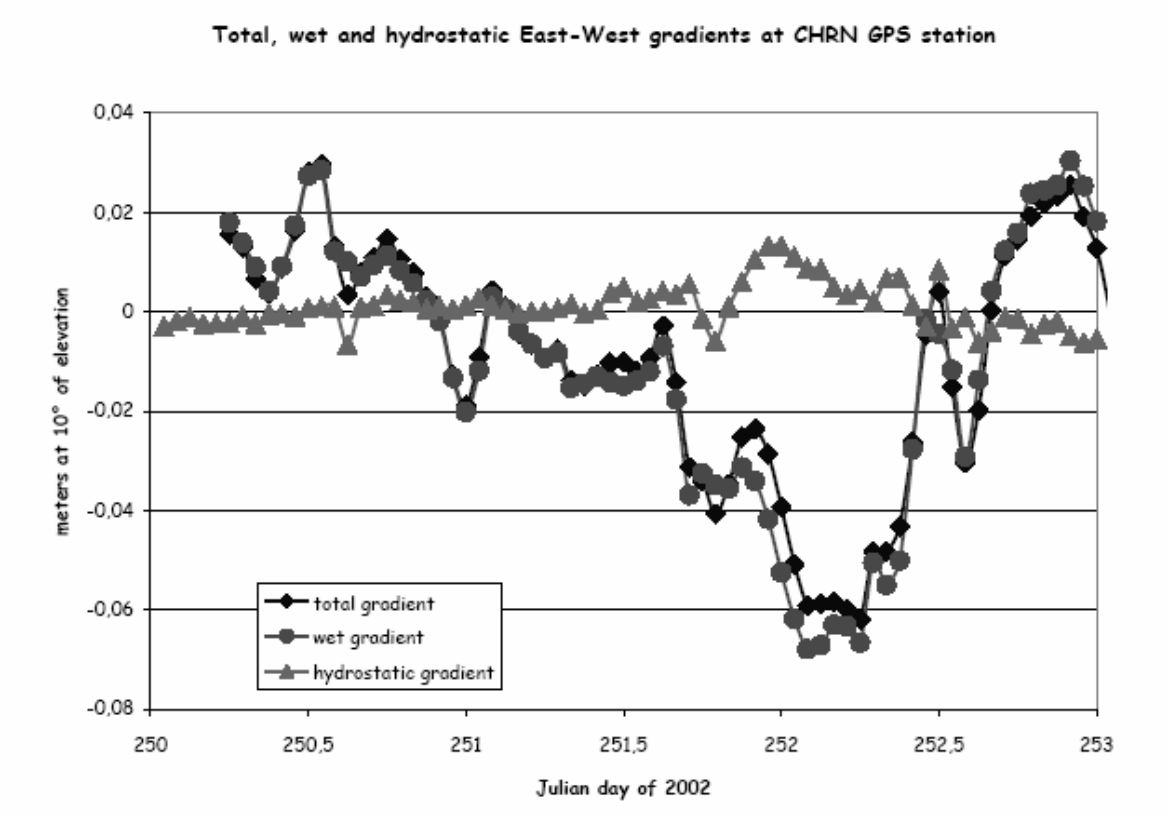

Figure 3:

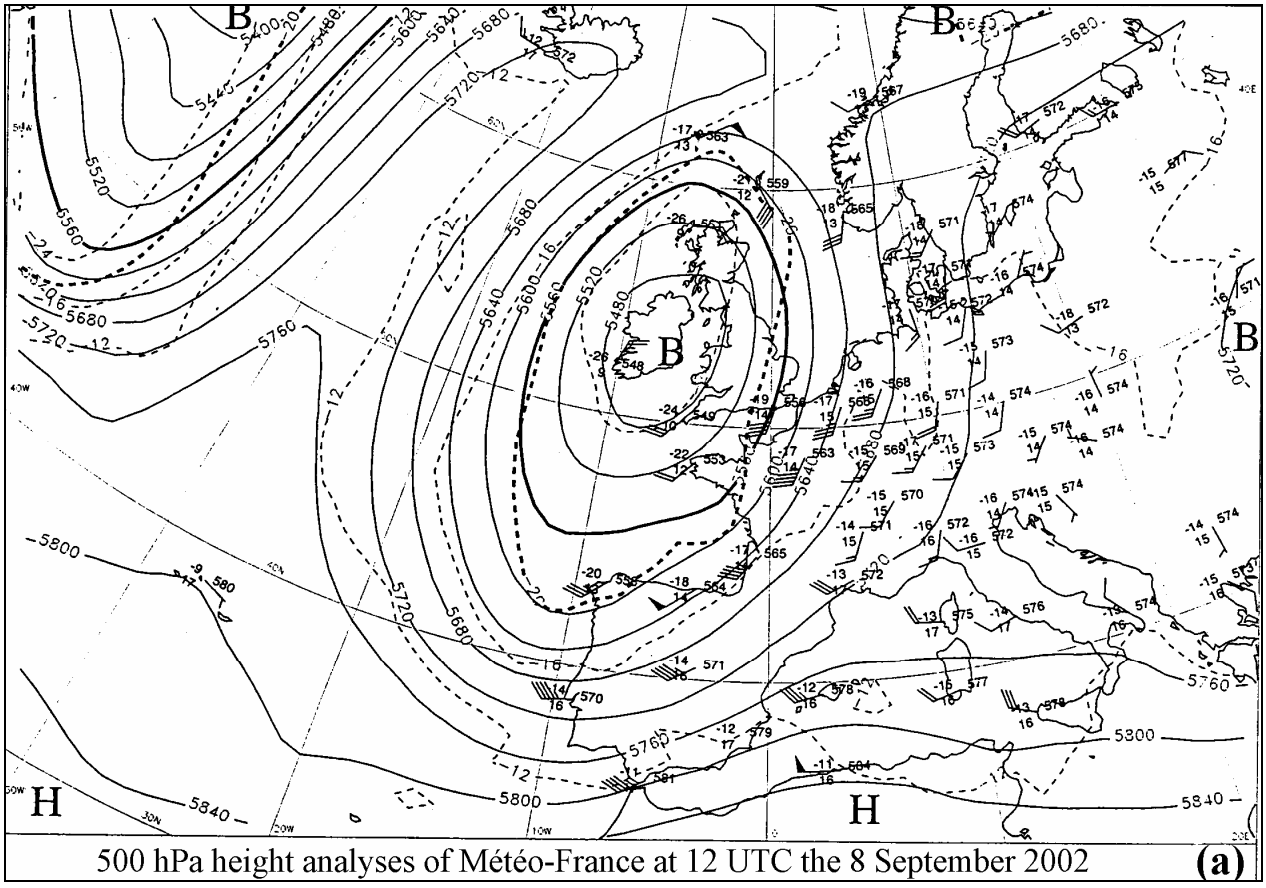

500 hPa height analyses of Météo-France at 12 UTC the 8 September 2002 **(a)**

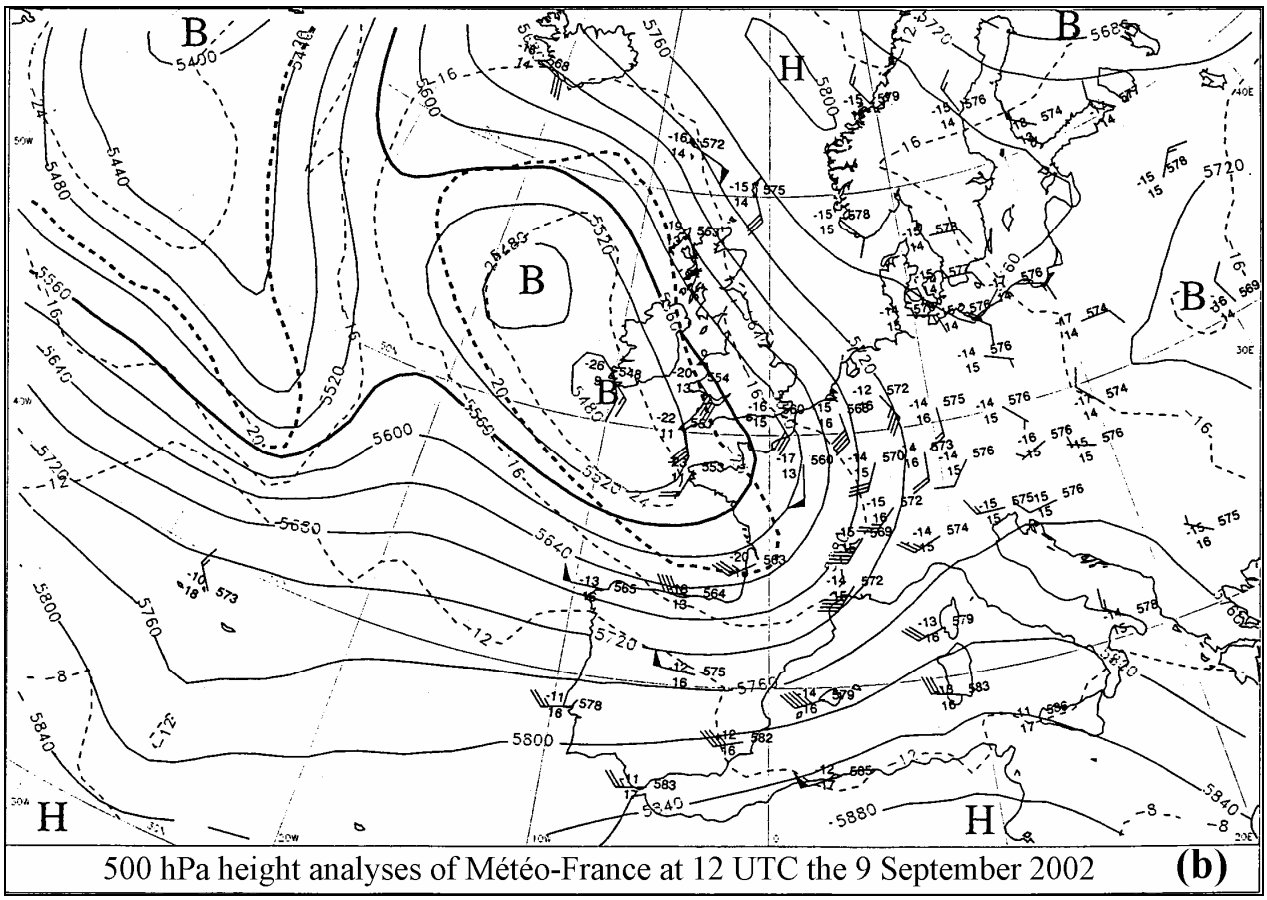

500 hPa height analyses of Météo-France at 12 UTC the 9 September 2002 **(b)**

Figure 4:

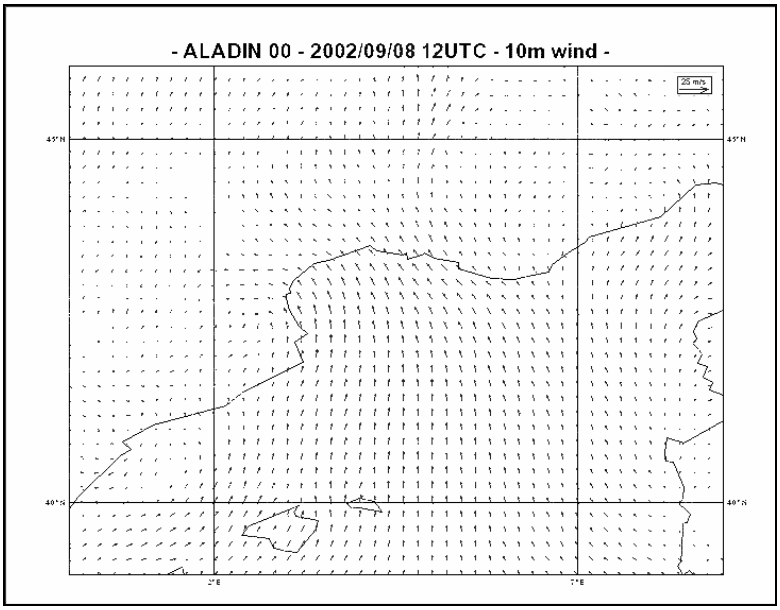
- ALADIN 00 - 2002/09/08 12UTC - 10m wind -
25 m/s

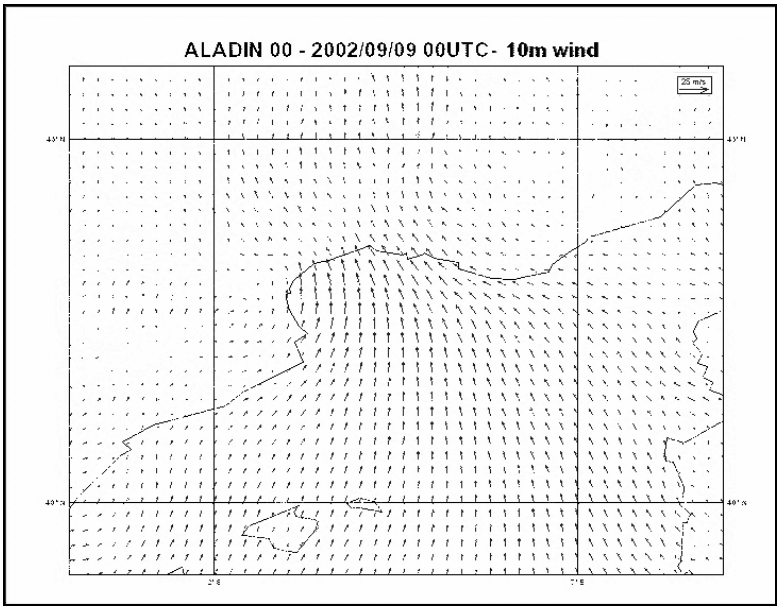
ALADIN 00 - 2002/09/09 00UTC - 10m wind
25 m/s

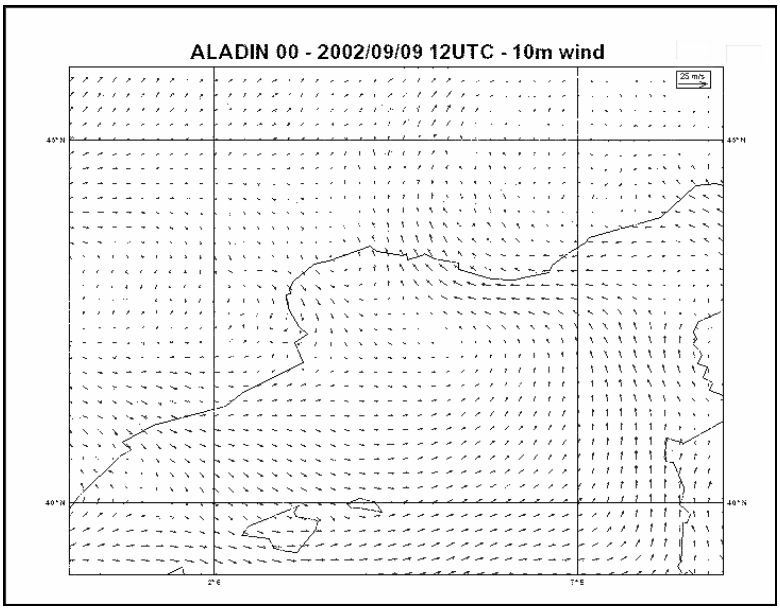
ALADIN 00 - 2002/09/09 12UTC - 10m wind
25 m/s

Figure 5:

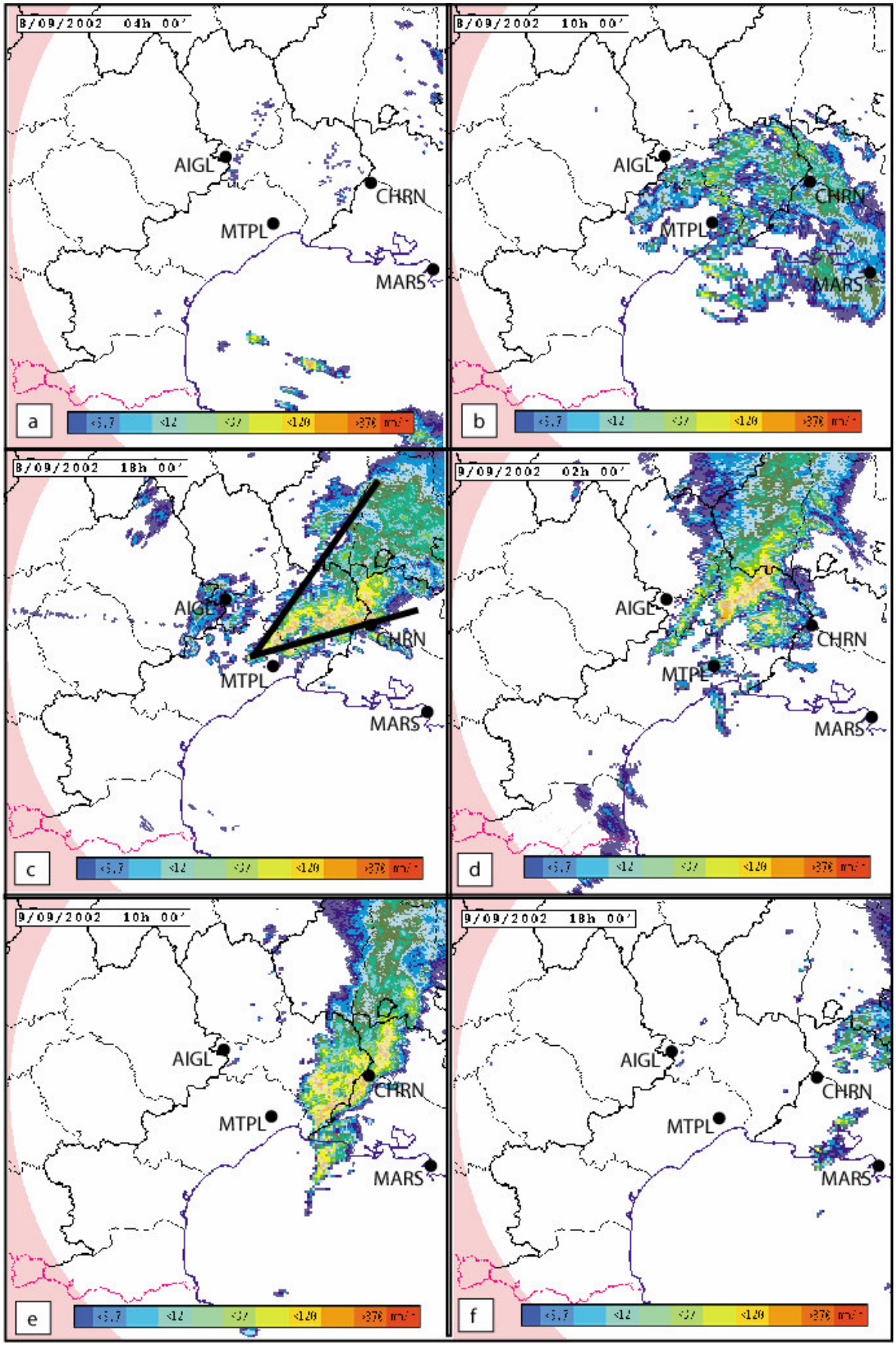
8/09/2002 04h 00'
AIGL
CHRN
MTPL
MARS
a
8/09/2002 10h 00'
AIGL
CHRN
MTPL
MARS
b
8/09/2002 18h 00'
AIGL
CHRN
MTPL
MARS
c
9/09/2002 02h 00'
AIGL
CHRN
MTPL
MARS
d
9/09/2002 10h 00'
AIGL
CHRN
MTPL
MARS
e
9/09/2002 18h 00'
AIGL
CHRN
MTPL
MARS
f

Figure 6:

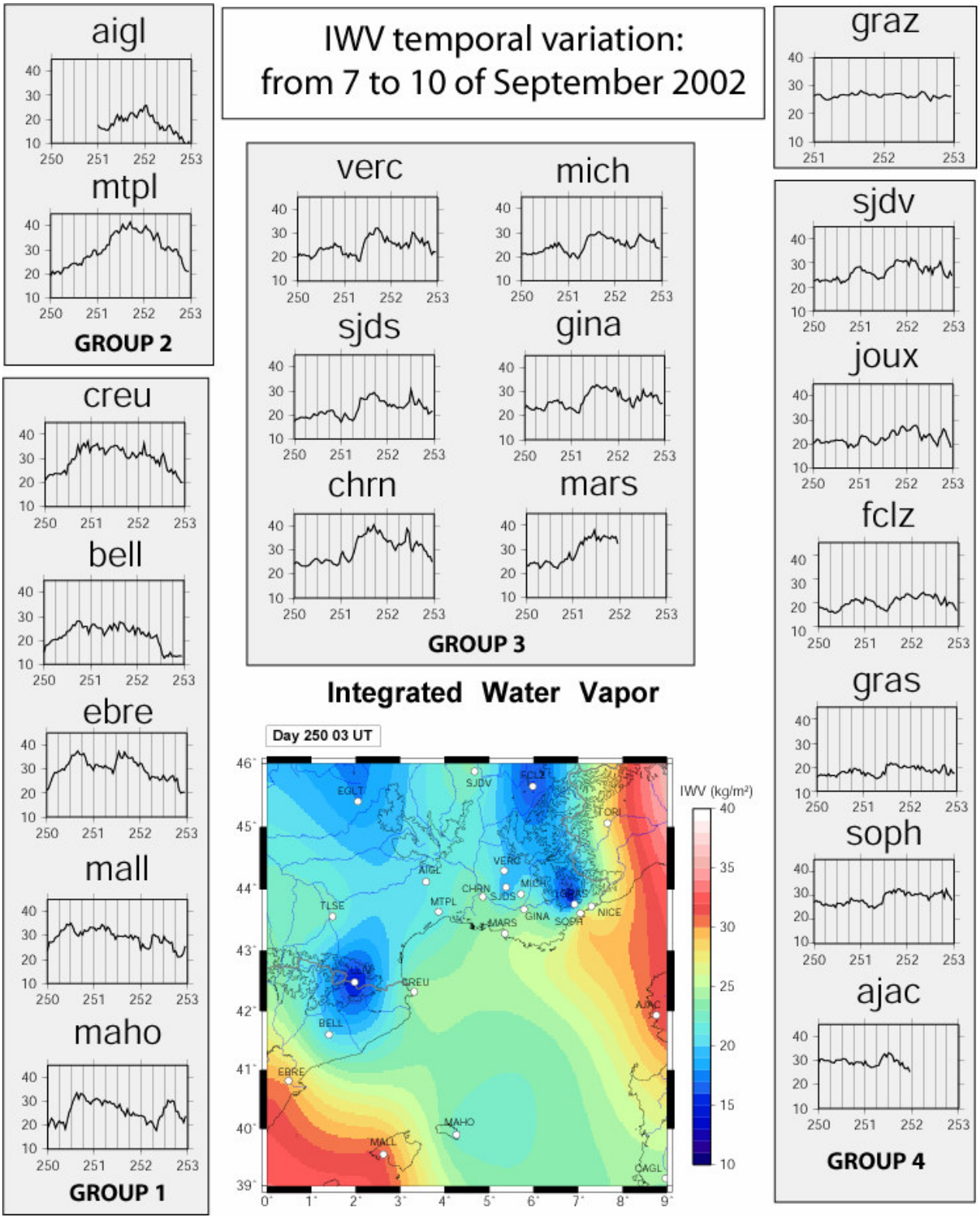
IWV temporal variation:
from 7 to 10 of September 2002
aigl
mtpl
GROUP 2
creu
bell
ebre
mall
maho
GROUP 1
verc
mich
sjds
gina
chrn
mars
GROUP 3
graz
sjdv
joux
fclz
gras
soph
ajac
GROUP 4
Integrated Water Vapor
Day 250 03 UT
IWV (kg/m²)
EGLT
SJDV
FCLZ
TORI
AIGL
VERC
MICH
CHRN
SJDS
GRAS
MTPL
TLSE
GINA
SOPH
NICE
MARS
CREU
AJAC
BELL
EBRE
MAHO
MALL
CAGL

Figure 7:

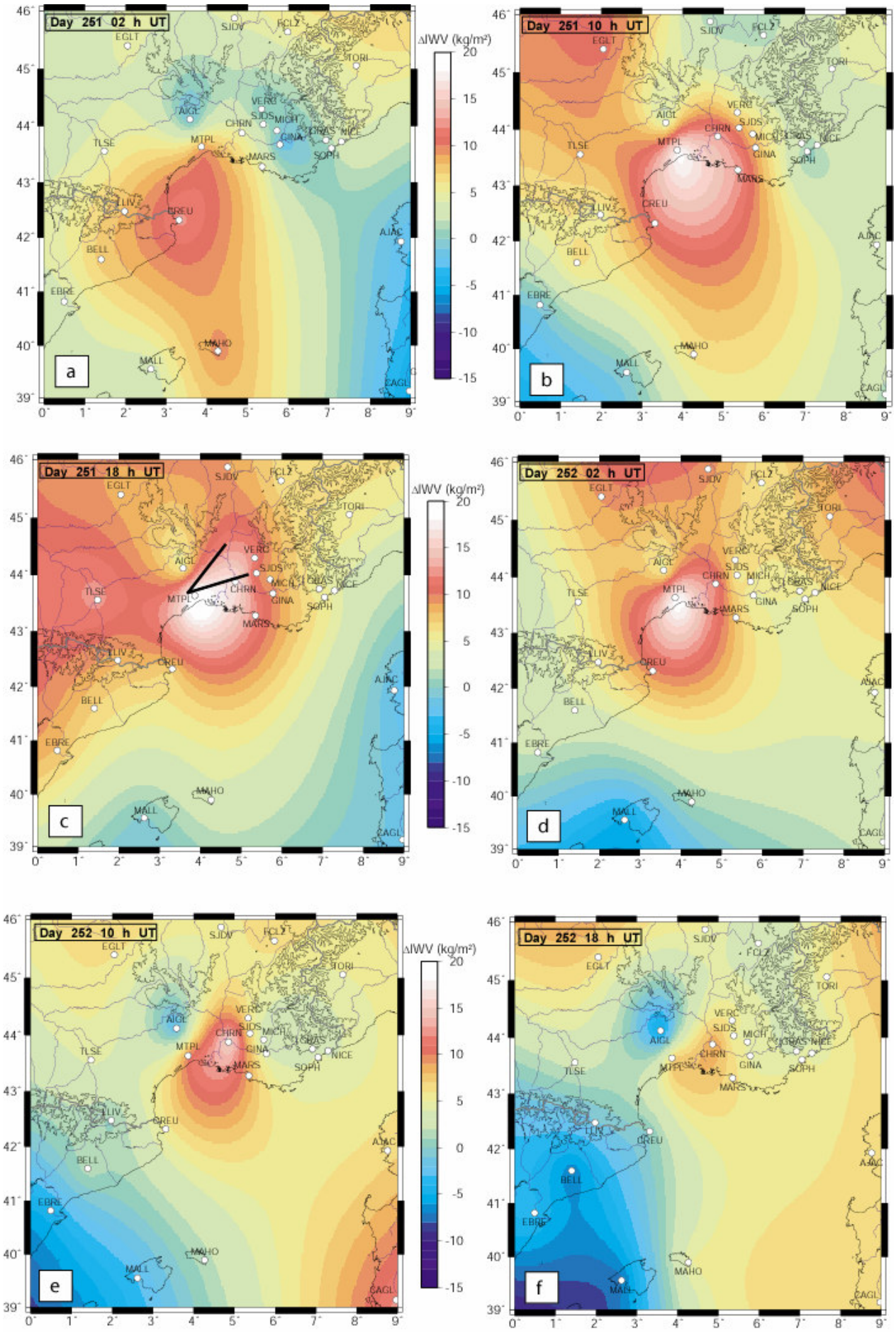
Day 251 02 h UT
Day 251 10 h UT
Day 251 18 h UT
Day 252 02 h UT
Day 252 10 h UT
Day 252 18 h UT
ΔIWV (kg/m²)
20
15
10
5
0
-5
-10
-15
a
b
c
d
e
f
EGLT
SJDV
FCLZ
TORI
VERC
AIGL
SJDS
MICH
CHRN
GINA
CRAS
NICE
SOPH
TLSE
MTPL
MARS
LIVI
CREU
AJAC
BELL
EBRE
MAHO
MALL
CAGL

Figure 8:

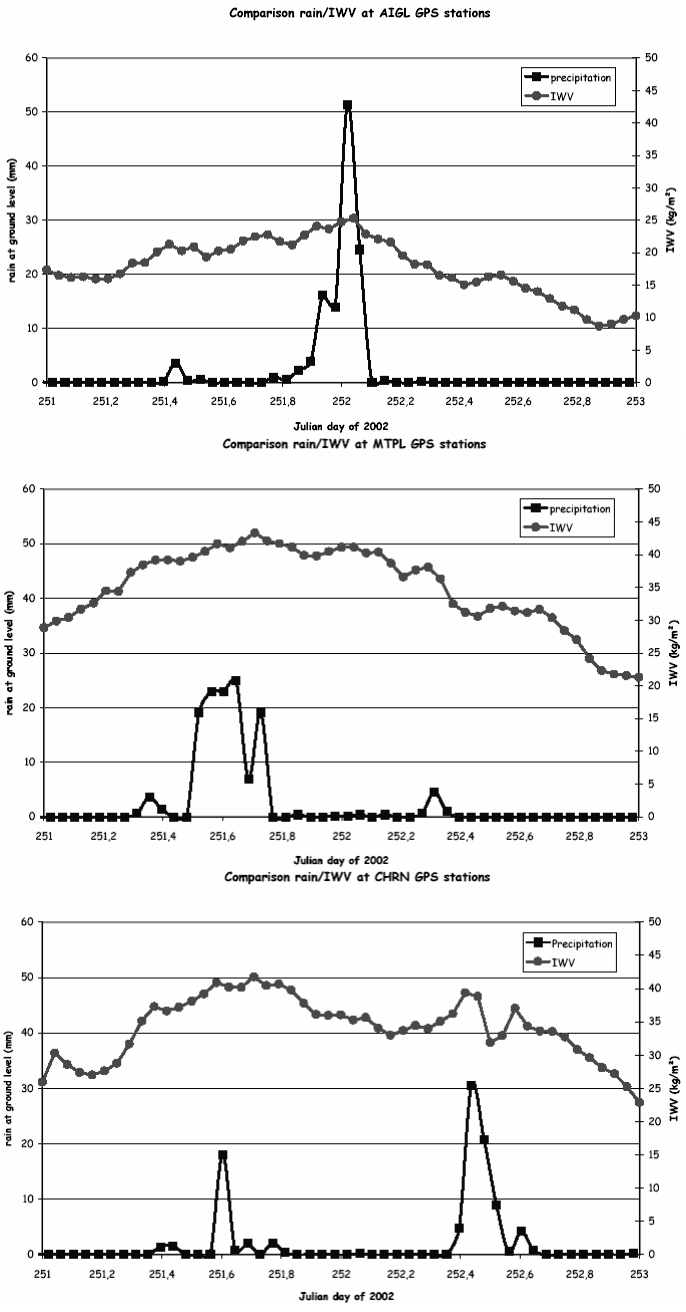
Comparison rain/IWV at AIGL GPS stations
precipitation
IWV
rain at ground level (mm)
IWV (kg/m²)
Julian day of 2002
Comparison rain/IWV at MTPL GPS stations
precipitation
IWV
rain at ground level (mm)
IWV (kg/m²)
Julian day of 2002
Comparison rain/IWV at CHRN GPS stations
Precipitation
IWV
rain at ground level (mm)
IWV (kg/m²)
Julian day of 2002

Figure 9.

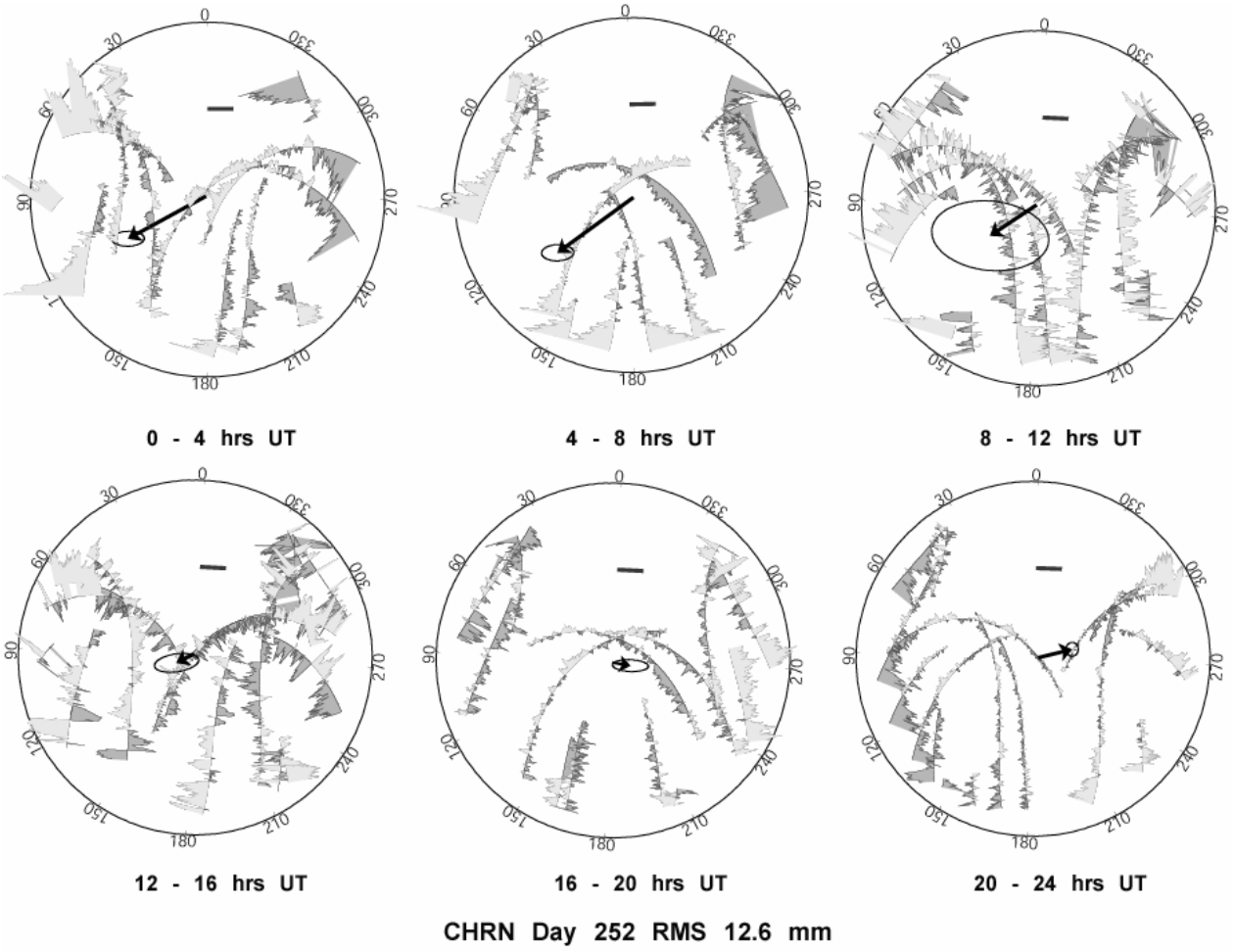
0 - 4 hrs UT
4 - 8 hrs UT
8 - 12 hrs UT
12 - 16 hrs UT
16 - 20 hrs UT
20 - 24 hrs UT
CHRN Day 252 RMS 12.6 mm

Figure 10:

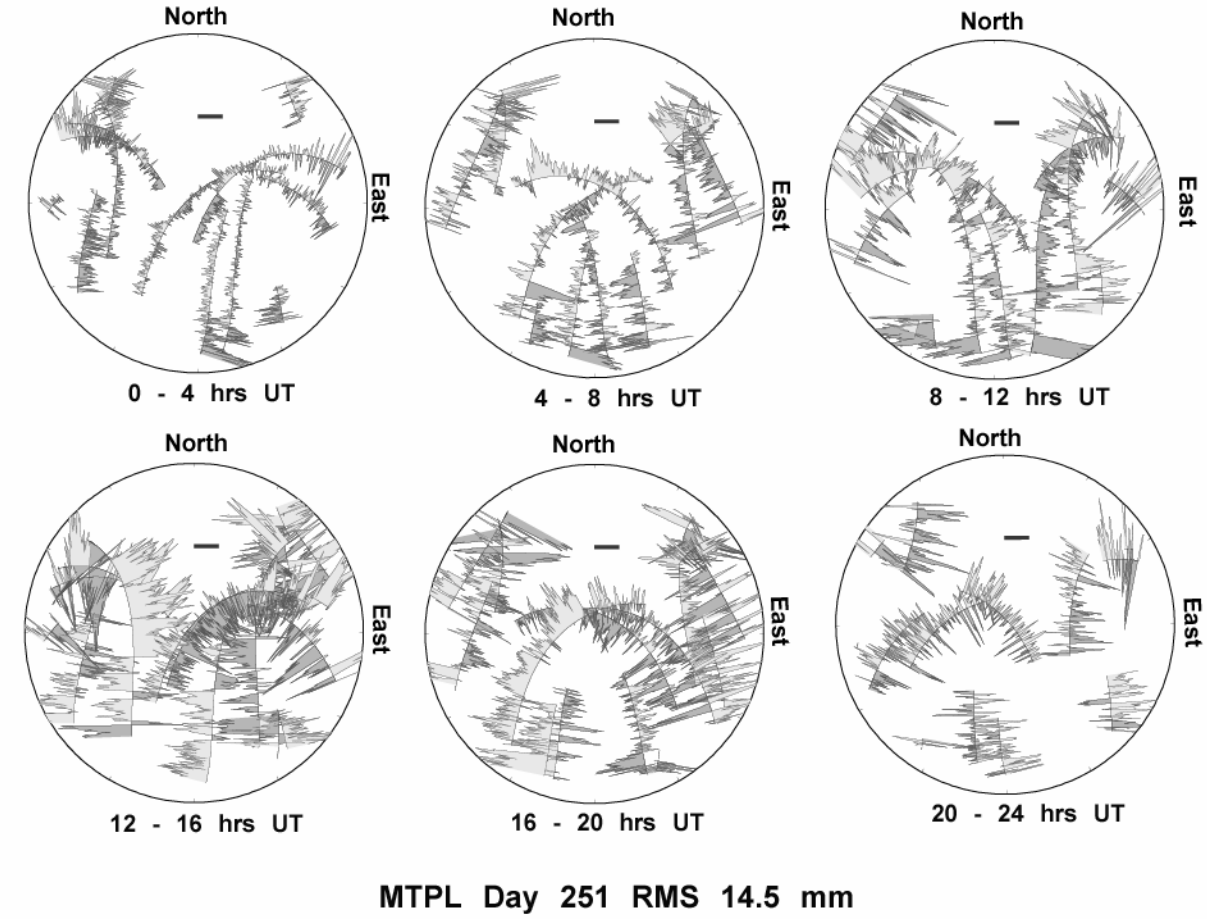
North
East
0 - 4 hrs UT
North
East
4 - 8 hrs UT
North
East
8 - 12 hrs UT
North
East
12 - 16 hrs UT
North
East
16 - 20 hrs UT
North
East
20 - 24 hrs UT
MTPL Day 251 RMS 14.5 mm